Biomaterials Science

ROYAL SOCIETY OF CHEMISTRY

PAPER

View Article Online
View Journal | View Issue

Cite this: *Biomater. Sci.*, 2022, **10**, 3309

Dopamine-derived nanoparticles for the protection of irradiation-induced intestinal injury by maintaining intestinal homeostasis†

Shuhan Jia,‡[a] Suhe Dong,‡[b] Heng Liu,‡[b] Huijie Yu,[b] Zhongmin Chen,[b] Sinian Wang,[b] Wei Li,[b] Renjun Peng,[b] Fengsheng Li,*[b] Qisheng Jiang*[b] and Jianjun Liu *[b]

Radiotherapy of abdominal and pelvic tumors almost inevitably injures the intestine by oxidative stress and causes inflammation. Regrettably, traditional radioprotective agents for irradiation (IR) induced intestinal injury suffer from challenges such as poor solubility, unsatisfactory bioactivity and undesired adverse reactions, which significantly limit their usefulness. Polydopamine nanoparticles (PDA-NPs) have shown promising potential in scavenging reactive oxygen species (ROS) and suppressing inflammation. In this study, PDA-NPs were prepared by a simple method and their physical properties were characterized. Mice received two doses of PDA-NPs by oral gavage 22 h apart, and were irradiated with X-rays 2 h after the last gavage. The protective effect of PDA-NPs and possible mechanisms of protection against IR-induced intestinal injury were explored. The results showed that PDA-NPs were spherical and well dispersed, with good shape uniformity, compact structure, good colloid dispersion stability, concentration-dependent light absorption, and accurate quantification. Importantly, PDA-NPs reduced mortality and prolonged the average survival time of mice after IR. Furthermore, PDA-NPs protected mice from IR-induced injury to crypt–villus units and maintained intestinal barrier function in the intestine. In particular, PDA-NPs significantly inhibited the depletion of $Lgr5^+$ intestinal stem cells (ISCs) and promoted cell regeneration after IR, which indicated that the regeneration ability of ISCs was maintained and the repair of intestinal structure and function was promoted. Finally, PDA-NPs significantly suppressed the apoptosis, inflammatory pyroptosis and DNA damage of intestinal cells induced by ionizing radiation. Altogether, our study suggested that PDA-NPs may have great potential in protecting the intestines from ionizing radiation damage.

Received 31st December 2021,
Accepted 26th April 2022

DOI: 10.1039/d1bm02026a

rsc.li/biomaterials-science

[a]*The Postgraduate Training Base of Jinzhou Medical University (The PLA Rocket Force Characteristic Medical Center), Beijing, China. E-mail: shuhan0418@163.com*
[b]*The PLA Rocket Force Characteristic Medical Center, Beijing, China. E-mail: lifs0624@163.com, jiangqisheng2020@163.com, jianjun.liu7599@outlook.com, wei_v76@126.com, pengrenjun001@163.com, wangsinian@126.com, hero_czhm@163.com, jie323@sina.com, liuheng0918@163.com*

†Electronic supplementary information (ESI) available: Fig. S1: HIEC cells were pretreated with 8 μg mL^{-1} PDA-NPs or 50 μM dopamine respectively, before 8 Gy IR. Cell viability was measured by the CCK-8 assay, $n = 3$. Data are expressed as mean ± SEM, $^*P < 0.05$, $^{**}P < 0.01$. Fig. S2: Zeta potential distribution of PDA-NPs. Fig. S3: Kaplan–Meier survival analysis of mice after exposure to 15 Gy ABI, $n = 10$. Fig. S4: Western blot analysis of the expression of apoptosis and inflammation proteins in 8 Gy irradiated HIEC cell lysates, $n = 3$. Fig. S5: Western blot analysis of the expression of pyroptosis proteins in 8 Gy irradiated HIEC cell lysates, $n = 3$. Fig. S6: The expression of TNF-α mRNA in 10 Gy tissue was detected by qPCR, $n = 3$. Data are expressed as mean ± SEM, $^*P < 0.05$, $^{**}P < 0.01$. Fig. S7: HIEC cell toxicity was monitored by the CCK-8 assay, $n = 3$. Data are expressed as mean ± SEM, $^*P < 0.05$, $^{**}P < 0.01$. Fig. S8: HIEC cells were pretreated with 8 μg mL^{-1} PDA-NPs before 8 Gy IR and cell viability was measured by the CCK-8 assay, $n = 3$. Data are expressed as mean ± SEM, $^*P < 0.05$, $^{**}P < 0.01$. Fig. S9: The ESR spectrum of $O_2^{\cdot-}$ with 8 μg mL^{-1} PDA-NPs in strong acid (pH = 2). Fig. S10: The ESR spectrum of DPPH with 8 μg mL^{-1} PDA-NPs in strong acid (pH = 2). See DOI: **https://doi.org/10.1039/d1bm02026a**

‡These authors contributed equally to this work.

1. Introduction

Radiotherapy is one of the main therapeutic approaches in cancer treatment clinically, and over half of cancer patients need to undergo radiotherapy in their fight against cancer.[1] Despite being effective and promising, local radiotherapy almost inevitably causes damage to adjacent healthy tissues.[2] When patients receive abdominal, pelvic or rectal radiotherapy, acute enterotoxic symptoms occur in 60–80% of them. They mainly manifest as a series of adverse symptoms, such as anorexia, nausea, vomiting, and abdominal distension. Some extreme cases of radiation enteropathy may even progress to septic shock and death.[3] Radiation enteropathy is a progressive, ischemic and fibrogenic pathological process and can be divided into early and delayed radiation enteropathies according to the time of onset.[4] The latter mainly manifests as angiosclerosis and progressive intestinal wall fibrosis, which is one of the core problems of cancer survivors. However, early radiation enteropathy (intestinal radiation toxicity) which occurs within 3 months after radiotherapy is more fatal. Unlike other types of tissue injury, radiation generates large amounts of

free radicals that not only cause immediate DNA damage but also ruin the structures of various biomacromolecules, promotes the death of rapidly proliferating crypt epithelial cells and induces a long-term acute inflammatory response in the lamina propria. Crypt cell death results in insufficient villous epithelial regeneration, mucosal barrier destruction, and mucosal inflammation.[2,5] Apoptosis has been used as a partial indicator of intestinal radiation toxicity.[6]

The intestinal epithelium is a single layer of tissue composed of repeated crypt–villus units. Considerable evidence has shown that mitotically active Lgr5$^+$ intestinal stem cells,[7,8] commonly known as crypt base columnar stem cells, are located in the proliferation niche of crypts. Each crypt has 4 to 6 ISCs, which can generate rapidly proliferating transit amplifying cells that can differentiate into intestinal cells, goblet cells and intestinal endocrine cells. All of these cells migrate upward, differentiate and are lost from the villus tip in average 5 days after birth.[7] Therefore, a single Lgr5$^+$ ISC can continuously generate all differentiated progeny cell types of the intestinal epithelium, including itself, and this characteristic is indispensable for maintaining normal homeostasis and intestinal regeneration.[9] In contrast, Paneth cells, as secretory intestinal epithelial cells, migrate down to the bottom of the crypt and last for up to 2 months,[10] which is crucial to maintain epithelial cell renewal. In addition, Paneth cells can generate lysozyme, which is also important for maintaining intestinal homeostasis.[11] Once the intestine is damaged by ionizing radiation, a large number of intestinal epithelial cells die, which triggers injury repair responses.[12] In mice, most epithelial cells are replaced within 3 to 5 days.[13] The high proliferation rate of intestinal epithelial cells, especially ISCs, makes the intestine one of the most vulnerable organs to radiation damage,[9] which is also the most important reason why it is necessary to develop protection against the toxicity and side effects of radiotherapy for patients with abdominal or pelvic tumors. At present, there is almost no treatment for radiation enteropathy.

Clinically, traditional antidiarrheal agents, antiemetic agents, spasmolytic agents and defoamers are the mainstay for treating acute enterotoxicity.[5] They can relieve the symptoms of radiation damage to the intestine to some extent but cannot fundamentally alleviate the injury to the intestine induced by IR. Studies have found that many small molecule compounds can protect the intestines from IR-induced injury by promoting the proliferation and differentiation of Lgr5$^+$ ISCs.[14] Regrettably, the majority of these agents suffer from challenges such as poor solubility, short circulation time, fast biological metabolism, unsatisfactory bioactivity and undesired adverse reactions, which significantly limit their usefulness. It is particularly urgent to develop high-efficiency and low-toxicity protective agents against IR-induced intestinal injury.

With the rapid development of nanotechnology, nanomaterials have emerged as potent paradigms with great promise in biomedicine.[15,16] Melanin is a class of biological macromolecular pigments present in most organisms, including bacteria, plants, animals and humans, and has been used as a therapeutic antioxidant and heat stabilizer for polymers due to its excellent free radical scavenging ability.[17] Eumelanins are the most common forms composed of indole monomers 5,6-dihydroxyindole-2-carboxylic acid or 5,6-dihydroxyindole-2-carboxylic acid, which is a very effective radiation protectant.[18] Although natural melanin can be significantly influenced by the biological and environment, melanin-like nanoparticles can only be gained through specific chemical reactions.[19] PDA-NPs, as nanoscale synthetic analogues of melanin, can be easily synthesized by a series of oxidation–polymerization processes from dopamine monomers.[19] PDA-NPs have excellent biocompatibility because of their similarity to melanin, which is naturally metabolized in skin.[20] Some studies have shown that PDA-NPs have good reactive oxygen scavenging ability and anti-inflammatory activity, which can be developed as an effective and safe agent, suggesting their potential as reactive oxygen scavengers and anti-inflammatory agents in inflammatory and oxidative stress-related diseases.[21–23] The antioxidative mechanisms of PDA-NPs as free radical scavengers in the human body can be categorized as follows: (i) dissipate radiation energy to prevent free radical formation; (ii) quench reactive species; and (iii) activate the defense mechanism *in vivo*.[24] Whether PDA-NPs could play a role in protecting against radiation enteropathy has not been reported in the literature.

In this study, PDA-NPs were prepared and characterized by various physical and chemical methods. Then, PDA-NPs were orally administrated to mice before total body irradiation (TBI), and the feasibility of using PDA-NPs as a protection against IR-induced intestinal injury and their possible mechanisms of action were explored. We confirmed that PDA-NPs showed favorable structural characteristics, reduced the mortality of mice, prolonged the average survival time of mice, improved the structure of crypt–villus units and maintained intestinal barrier function after IR. In particular, PDA-NPs ameliorated the depletion of Lgr5$^+$ ISCs and promoted the repair of intestinal structure and function. Moreover, PDA-NPs suppressed apoptosis and pyroptosis and alleviated DNA damage induced by ionizing radiation. All in all, our study suggested that PDA-NPs may be developed as a potential radioprotective agent against IR-induced intestinal damage.

2. Materials and methods

2.1 Reagents

Following reagents were purchased from indicated sources: dopamine hydrochloride (Abmole Bioscience, China); immunosorbent assay kit (Sinbestbio, China); antibodies Ki67, lysozyme, ZO-1 and villin (Servicebio, China); antibodies TNF-α, IL-6, caspase-1, GSDMD (Abcam, USA); FITC-dextran solution (Thermo Scientific, China); antibodies caspase-3, Bax, BCL-2, AIM2, IL-18, IL-1β, and 8-hydroxy-2-deoxyguanosine (8-OHdG) (Cell Signaling Technology, USA); antibody against GAPDH (Proteintech, China); secondary antibodies (Abcam, Cambridge, USA); BCA protein assay kit (Beyotime, China);

polyvinylidene fluoride membrane (Bio-Rad, USA); Tunel staining kit (Servicebio, China); penicillin and streptomycin (Gibco, USA); fetal bovine serum (Gibco, USA); TRIzol (Sigma, USA); ROS assay kit (GeneCopoeia, USA); MDA assay kit (Beyotime Biotechnology, China); PrimeScript RT Master Mix (Takara, Japan); xanthine (Solarbio, China); DPPH (Yuanye Biotechnology, China); xanthine oxidase (Yuanye Biotechnology, China); and DMPO (Yuanye Biotechnology, China).

2.2 Animals

Male C57BL/6J mice aged 6–8 weeks (average weight approximately 20 g) were purchased from SPF Biotechnology Co., Ltd (Beijing, China). All experimental procedures were conducted in accordance with the Guidelines for the Care and Use of Laboratory Animals (8th Edition, National Academy of Sciences Press, Washington, D.C., 2011) and approved by the Animal Care and Use Committee of the IRM, CAMS Institution (License No. 20190010). Animals were cared for according to the guidelines of China's National Animal Welfare Law.

2.3 Irradiation and treatment

Mice were irradiated with X-ray (KUBTEC, USA) at a dose rate of 1.0 Gy min^{-1} (225 kV, 13.2 mA). Mice were exposed to 7.5 Gy TBI and 15Gy abdomen irradiation (ABI) for survival analysis, 7.5 Gy for fecal collection and 10 Gy TBI for all the other experiments. The mice were randomly divided into the following two groups: irradiation only and IR plus PDA-NP treatment. Mice in the IR plus PDA-NPs group received 50 mg kg^{-1} PDA-NPs by gavage 24 h and 2 h before IR. Mice in the control group and IR group received a vehicle. Human intestinal epithelial cells (HIEC) were treated with 8 μg mL^{-1} PDA-NPs before IR with X-ray at 8 Gy.

2.4 Synthesis and characterization of PDA-NPs

For the synthesis of PDA-NPs, 90 mg of dopamine hydrochloride was dissolved in 45 mL of ultrapure water, stirred and heated to 50 °C, and 380 μL of 1 mol L^{-1} NaOH was immediately added. After reaction for 6 h, the solution was centrifuged at 11 000 rpm (25 min, 4 times) to remove excess unreacted reactants. The precipitate was collected and dissolved in ultrapure water at 4 °C for future use. The morphology of the PDA-NPs was observed by scanning electron microscopy (SEM, SU8230, Hitachi, Japan) and transmission electron microscopy (TEM, H-7500, Hitachi, Japan). The hydrodynamic size and zeta potential of PDA-NPs were measured using a dynamic light scattering instrument (Zetasizer Nano ZS90, Malvern, UK). A UV-vis spectrometer (Cary60, Agilent Technologies, USA) was used to evaluate the optical absorption spectrum of the nanoparticles at different concentrations. Fourier transform infrared spectroscopy (FT-IR, IR-Affinity-1S, Shimadzu, Japan) was used to detect the functional groups on the nanoparticles.

2.5 ESR assay

Electron spin resonance (ESR 5000, Bruker, GER) was used to record the characteristic spectrum of DMPO-OH. A reaction mixture of 400 mmol L^{-1} 5,5-dimethyl-1-pyrroline-*N*-oxide (DMPO), 0.4 mmol L^{-1} ferrous sulfate, deionized water (pH 4.5), and 10 μL of 4% H_2O_2 was quickly prepared and absorbed into a quartz capillary. After reaction for 30 s, the ESR spectrum was scanned between 330 mT and 340 mT. To evaluate the ability of PDA-NPs to scavenge hydroxyl radicals ($^{\bullet}OH$) instantaneously produced by the Fenton reaction, PDA-NPs with different concentration gradients were added to the Fenton reaction system individually, captured by DMPO, and recorded by ESR.

Superoxide anions ($O_2^{\bullet-}$) were generated by the reaction of xanthine and xanthine oxidase, and captured by DMPO. 100 mmol L^{-1} DMPO solution, 0.9 mmol L^{-1} DETAPAC aqueous solution, 560 mmol L^{-1} xanthine (Xan) aqueous solution, distilled water, and 56 U mL^{-1} xanthine oxidase (XOD) aqueous solution were prepared for subsequent experiments. 10 μL of each of the above 5 reagents were taken in sequence. They were injected into an EP tube, mixed well and quickly put into a quartz capillary for determination. After 30 s of reaction, the ESR spectrum was scanned between 330 mT and 340 mT. This was followed by replacing distilled water with 8 μg mL^{-1} PDA-NPs and repeating the above steps. HCl (pH = 2) was prepared to simulate the gastric acid environment *in vitro*. 8 μg mL^{-1} PDA-NPs was dispersed in this system for 2 h before the free radical scavenging assay to test the stability and free radical scavenging ability of PDA-NPs under acidic conditions.

2×10^{-3} mol L^{-1} of 1,1-diphenyl-2-picrylhydrazine (DPPH) solution and distilled water were prepared for subsequent experiments. 20 μL of each of the above two reagents was injected into an EP tube, and then mixed quickly into a quartz capillary tube. After 30 s of reaction, the ESR spectrum was scanned between 330 mT and 340 mT. This was followed by replacing distilled water with 8 μg mL^{-1} PDA-NPs and repeating the above steps. HCl (pH = 2) was prepared to simulate the gastric acid environment *in vitro*. 8 μg mL^{-1} PDA-NPs was dispersed in this system for 2 h before the free radical scavenging assay to test the stability and free radical scavenging ability of PDA-NPs under acidic conditions.

2.6 Photoacoustic imaging (PAI)

PDA-NPs were imaged at 700, 750, 800, 850, 900 nm using a photoacoustic (PA) computerized tomography scanner (Endra Nexus 128, Endra Life Sciences, USA). Quantitative information was obtained by the Image J software. Similarly, 200 μL of PDA-NPs (5 mg mL^{-1}) was given by gavage to the mice. Photoacoustic imaging was performed on the mice at a specific time point at 800 nm.

2.7 Mouse feces assay

The mice were irradiated at 7.5 Gy. On days 0, 1, 3, and 7, three mice from each group were randomly selected and placed in a metabolic cage, and the amount of feces the mice

produced within 2 h was measured; the feces were collected, morphology was observed, and the number and weight of feces were recorded.

2.8 Histological and immunohistochemical assay

On days 1 and 3.5 after TBI, the intestines of mice were collected and fixed with formaldehyde (4%). The intestines were stained with H&E, hematoxylin and periodate Schiff. Samples were also analyzed by immunohistochemistry using antibodies against Ki67, lysozyme, ZO-1, villin and 8-OHdG followed by appropriate secondary antibodies. Slides were observed using an optical microscope (Eclipse E200, Nikon, JPN) and the ImageJ 1.53 software. In addition, slides of 8-OHdG were observed under a fluorescence microscope. For Tunel staining, sections were processed according to the manufacturer's protocol.

2.9 Fluorescence *in situ* hybridization (FISH) probe

Paraffin-embedded intestinal sections prepared from mice as described above were antigen repaired, digested and thoroughly washed with PBS. The prehybridization solution was applied dropwise and incubated at 37 °C for 1 h. Then, the hybridization solution containing the $Lgr5^+$ probe was applied dropwise and hybridized at 42 °C in an incubator overnight. The nuclei were stained with DAPI. The sections were observed under an upright fluorescence microscope (Eclipse Ci, Nikon, JPN), and images were captured.

2.10 FITC-dextran permeability assay

On the 3rd day after TBI, mice were gavaged with 0.6 mg per g body weight FITC-dextran solution (10 kDa). Four hours later, mice were bled from the retroorbital sinus and serum was prepared. The fluorescence intensity of the sample measured at 490 nm in a microplate reader (Varioskan LUX, Thermo Fisher, USA) was used to determine the serum level of FITC-dextran in each treatment group.

2.11 DAO activity assay

On the 1st day after TBI, a colorimetric sandwich enzyme-linked immunosorbent assay kit was used to determine the DAO activity in serum. All samples were measured in duplicate using a commercial assay kit.

2.12 Malondialdehyde (MDA) assay

The lipid peroxidation of intestines was evaluated by measuring the MDA concentrations using the thiobarbituric acid (TBA) method, which is based on the reaction of TBA and MDA. MDA content was calculated by the absorbance of TBA reaction substance at 532 nm.

2.13 RT-qPCR

Total RNA was extracted from intestines with TRIzol, then reverse-transcribed into cDNA using PrimeScript RT Master Mix. cDNA solution was amplified on a PCR instrument (CFX96, Bio-Rad, USA). The CT values were subsequently analysed based on the Bio-Rad CFX Manager software using $2^{-\Delta\Delta Ct}$ method. The sequences of primers used were as follows: TNF-α

Forward: GGTGCCTATGTCTCAGCCTCTT
Reverse: GCCATAGAACTGATGAGAGGGAG.
GAPDH
Forward: GCCATCACTGCCACTCAGAA
Reverse: GGC ATGTCAGATCCACAACG

2.14 Protein extraction and western blot assay

Mouse intestinal tissues and HIEC cells were fully ground and lysed with RIPA lysis buffer containing protease and phosphatase inhibitors at 4 °C. The protein concentration was measured using the BCA protein assay kit. Twenty micrograms of protein was separated by 10% SDS–PAGE and transferred to a polyvinylidene fluoride membrane. The membrane was blocked at room temperature with 5% skimmed milk in Tris-buffered saline for 1 h and then incubated with the corresponding antibodies overnight at 4 °C. The antibodies against TNF-α, IL-6, caspase-1, GSDMD, caspase-3, Bax, BCL-2, AIM2, IL-18, IL-1β, and GAPDH were used. After washing with TBST three times (10 minutes each time), the membrane was incubated with the secondary antibody at room temperature for 1 h and then washed with TBST three times (10 minutes each time). Protein bands were detected using a gel imaging system (Bio-Rad, USA).

2.15 Cell culture

HIEC cell line was purchased from Eallbio Life Sciences (Beijing, China). The cells were cultured in RPMI 1640 medium containing 10% fetal bovine serum, 100 U mL^{-1} penicillin and 100 mg mL^{-1} streptomycin. The cells were cultured in an incubator at 37 °C and 5% CO_2.

2.16 Viability of HIEC

HIEC cells were assessed by CCK-8 assay. Briefly, HIEC cells (8×10^3 cells per well) were treated with different concentrations of PDA-NPs before plating in 96-well plates, and the Maestro Z impedance system (Maestro Z, Axion BioSystmes, USA) was used for testing.

2.17 Cellular ROS assay

HIEC cells were seeded in 6-well plates, cultured overnight, and treated with 0 or 8 μg mL^{-1} PDA-NPs for 12 h and 2 h before 8 Gy IR. The ROS in HIEC cells were determined using the ROS kit based on the manufacturer's instructions. Briefly, treated HIEC cells were washed twice with calcium and magnesium-free balanced salt solution. The cells were incubated with 10 μmol L^{-1} H2DCFDA for 30 min at 37 °C and subsequently washed with PBS. Cellular ROS generation was determined using a flow cytometer at 495/529 nm.

2.18 Statistics analysis

Statistical analysis was performed using GraphPad Prism 7 (San Diego, USA). All data are expressed as the mean ± standard error. A *t* test was used to compare two independent samples, and ANOVA was used for comparisons among mul-

tiple groups. $P < 0.05$ was considered to be statistically significant.

3 Results and discussion

3.1 Synthesis and characterization of PDA-NPs

Because of the positive impact of nanomaterials on human health, their application in the biomedical field is drawing more attention. In recent years, polymer-based nanomaterials have been used to improve the poor stability and low bioavailability of small molecule compounds. Compared to traditional small molecule agents, nanomaterials significantly increase the specific surface area of drugs, improve organ targeting, and enhance drug efficacy and bioavailability.[25] At present, some agents and polymers are made into nanoparticles, which are used to prevent and treat various diseases, including drug delivery, cancer treatment, antibacterial materials, and potential vaccine adjuvants.[26] Some nanomaterials with inherent antioxidant properties have become free radical scavengers with good biocompatibility.[27] It has been reported that melanin nanoparticles are effective radioprotective agents that can prevent IR-induced damage to hematopoiesis and DNA in mice and have the ability to scavenge free radicals and maintain immunoregulation.[28] We demonstrated that PDA-NPs had a radioprotective effect *in vitro*, while its dopamine monomer behaved satisfactorily (Fig. S1†). The special structure of dopamine determines its key role in various biological processes. Different functional groups in its structure, such as amine, imine and catechol groups, can be used as the starting point of various conjugation reactions. Under alkaline conditions, catechol groups in dopamine undergo rapid oxidation to form quinone groups, and sulfhydryl groups or amine groups can form PDA-NP nanoparticles through a Michael addition or Schiff base reaction.[29] However, the effect of PDA-NPs on intestinal injury induced by ionizing radiation is still unclear. In our study, PDA-NPs were easily prepared by the oxidation and self-polymerization of dopamine under alkaline conditions (Fig. 1A). The color of the reaction solution gradually changed from transparent to light yellow and finally to dark brown. DLS data showed that the average hydrodynamic size of PDA-NPs was 210.3 nm (Fig. 1B), with a polydispersion index of 0.074. The zeta potential of PDA-NPs was −18.9 mV (Fig. S2†), which was crucial for maintaining good colloid dispersion stability. Representative SEM and TEM images shown in Fig. 1C and D indicated that the as-prepared PDA-NPs were spherical and well dispersed, showed good shape uniformity and close-packed structure, and their diameters were between 107 nm and 183 nm. Elemental analysis of PDA-NPs indicated that the rates of carbon and oxygen atoms accounted for 75.43% and 18.07%, respectively (Fig. 1E). UV-vis absorption spectra of PDA-NP solutions showed concentration-dependent optical absorption in the range of 300–900 nm (Fig. 1F). The absorption spectra at 800 nm showed a linear relationship with PDA-NP concentration (Fig. 1G). This property can be used for precise quantification of the nanoparticles. The results of the Fourier transform infrared (FT-IR) spectra provided additional evidence of the successful formation of PDA-NPs. Both dopamine and PDA-NPs exhibited a broad stretching at around 3650 cm^{-1} and 3100 cm^{-1} for N–H, O–H and NH_2. However, in the PDA-NP spectrum, the strong absorption peak centered at 1610 cm^{-1} was low in the dopamine spectrum, which may be due to the formation of dopamine oxidation and indole-related structures after self-polymerization.[19,30] Between 800 cm^{-1} and 700 cm^{-1}, the absorption bands of PDA-NPs were significantly weaker than that of dopamine, indicating a reduction in aromatic hydrogen and aromatic nucleus, as well as the successful formation of polymer structures in PDA-NPs (Fig. 1H). PAI has been applied in biomedical research of nanomaterials because of its non-invasive feature. Owing to the specific structure and the higher photothermal conversion efficiency, PDA-NPs showed excellent PA contrast abilities.[31] Therefore, PAI was performed to monitor the photoacoustic signals of PDA-NPs at 700, 750, 800, 850, and 900 nm *in vitro* (Fig. 1I). Quantitative observation showed that PDA-NPs had the strongest fluorescence signal at 800 nm (Fig. 1J). Therefore, we chose this wavelength for *in vivo* imaging observation of the intragastric administered mice.

3.2 PDA-NPs improved survival and alleviated intestinal injury induced by TBI in mice

High-quality and auxiliary imaging techniques of PAI can precisely and effectively achieve the visual observation of the absorption of PDA-NPs in the intestines of mice, playing the role of a "navigator". PAI was performed at 0, 2, 4, 6 h after intragastric administration. The results showed that there was low PA signal in mice without the administration, which ensured that high contrast images from biological imaging were free of background noise. High PA signals were observed at 800 nm after the administration, and the PA signal intensity was the highest 2 h after intragastric administration, then the PA signal decreased successively at 4 h and 6 h (Fig. 2A). Meanwhile, TEM showed that PDA-NPs was absorbed in the intestines of mice 2 h after intragastric administration (Fig. 2B), which directly indicated PDA-NPs can be absorbed into intestinal epithelium for the prevention of radiation damage. To evaluate the radioprotective effect of PDA-NPs on the mice irradiated with a lethal dose, 50 mg kg^{-1} PDA-NPs was administered orally 24 h and 2 h before TBI (Fig. 2C), and the mice were monitored for up to 30 days. All mice in the IR group died within 11 days, while 2 mice in the IR + PDA-NPs group survived until the 30th day, which significantly increased the survival rate to 20% and increased the average survival time after TBI from 6 days (IR group) to 10.2 days (IR + PDA-NPs group; $P < 0.001$) (Fig. 2D). Similarly, we treated mice with 15 Gy ABI, and PDA-NP-treated group had the same significant effect (IR + PDA-NPs group; $P < 0.001$) (Fig. S 3†). After IR, the villus of the intestine may be ruined and shortened to varying degrees. The depletion and attenuation of crypt epithelium and villous epithelial cells disrupts epithelial cell homeostasis and epithelial tight junction integrity. Irradiation

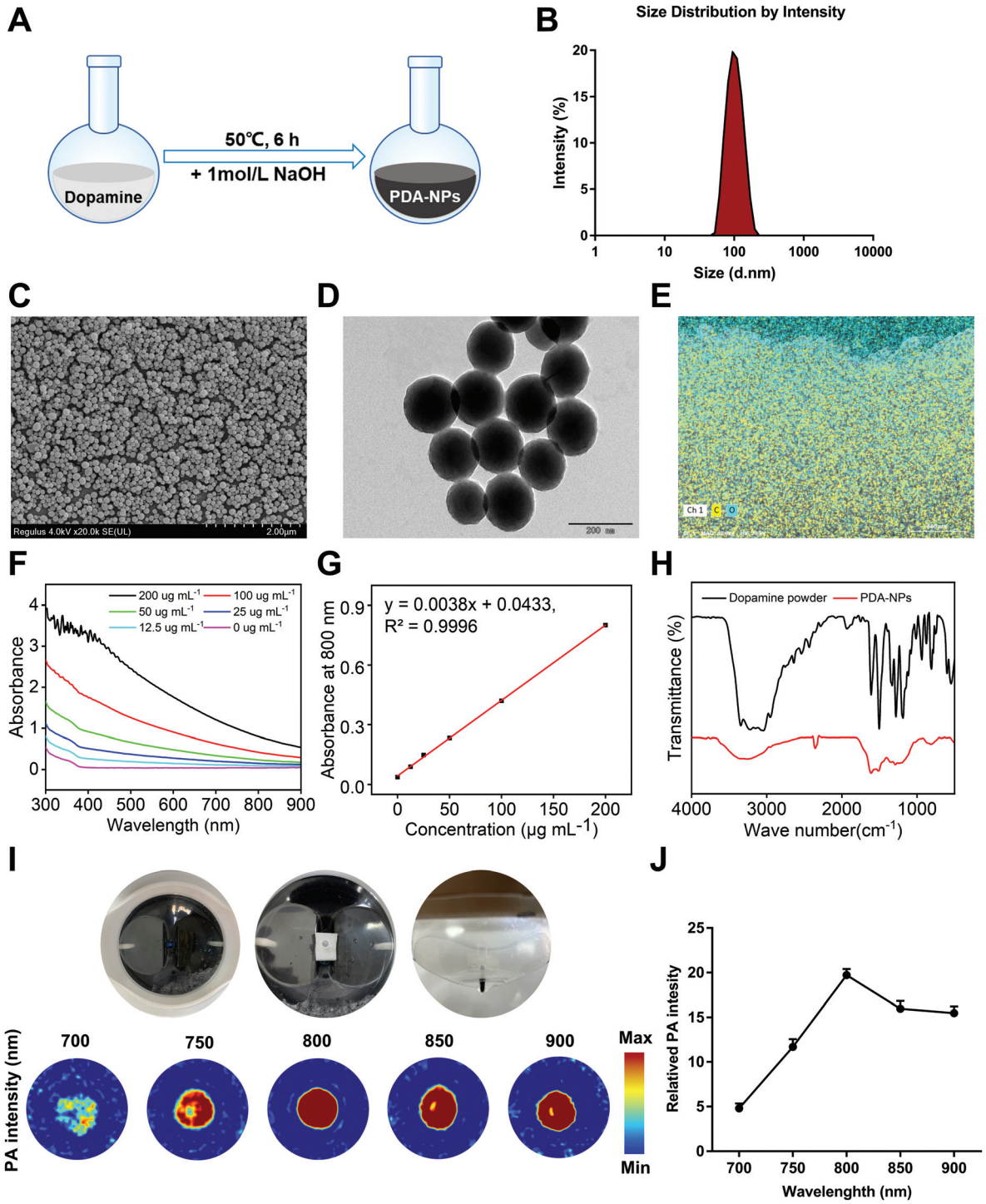

Fig. 1 Characterization and free radicals scavenging of PDA-NPs. (A) The pattern of PDA-NP synthesis. (B) Size distribution by intensity of PDA-NPs. (C and D) SEM and TEM images of PDA-NPs. Scale bar: 2 μm (left) and 200 nm (right). (E) The responding elemental mapping images in SEM (C, O). (F) The characteristic peaks of FTIR both dopamine and PDA-NPs. (G) UV-vis absorption spectrum of PDA-NPs with different mass concentrations. (H) The linearity for absorbance at 800 nm in different concentrations of PDA-NPs. (I) The picture of PA imaging device and PA imaging of PDA-NPs at different wavelengths. (J) Statistics of PA imaging of PDA-NPs at different wavelengths. Data were expressed as Mean ± SEM, * $P < 0.05$, ** $P < 0.01$.

can cause pathophysiological damage, including vacuolization of epithelial cells, shortening of villi and infiltration of inflammatory cells.[32] To determine the protective effect of PDA-NPs on intestinal radiation injury in mice, we investigated general changes in the intestine. Three days after IR, IR reduced the contents of the intestine, caused intestinal contents to leak to

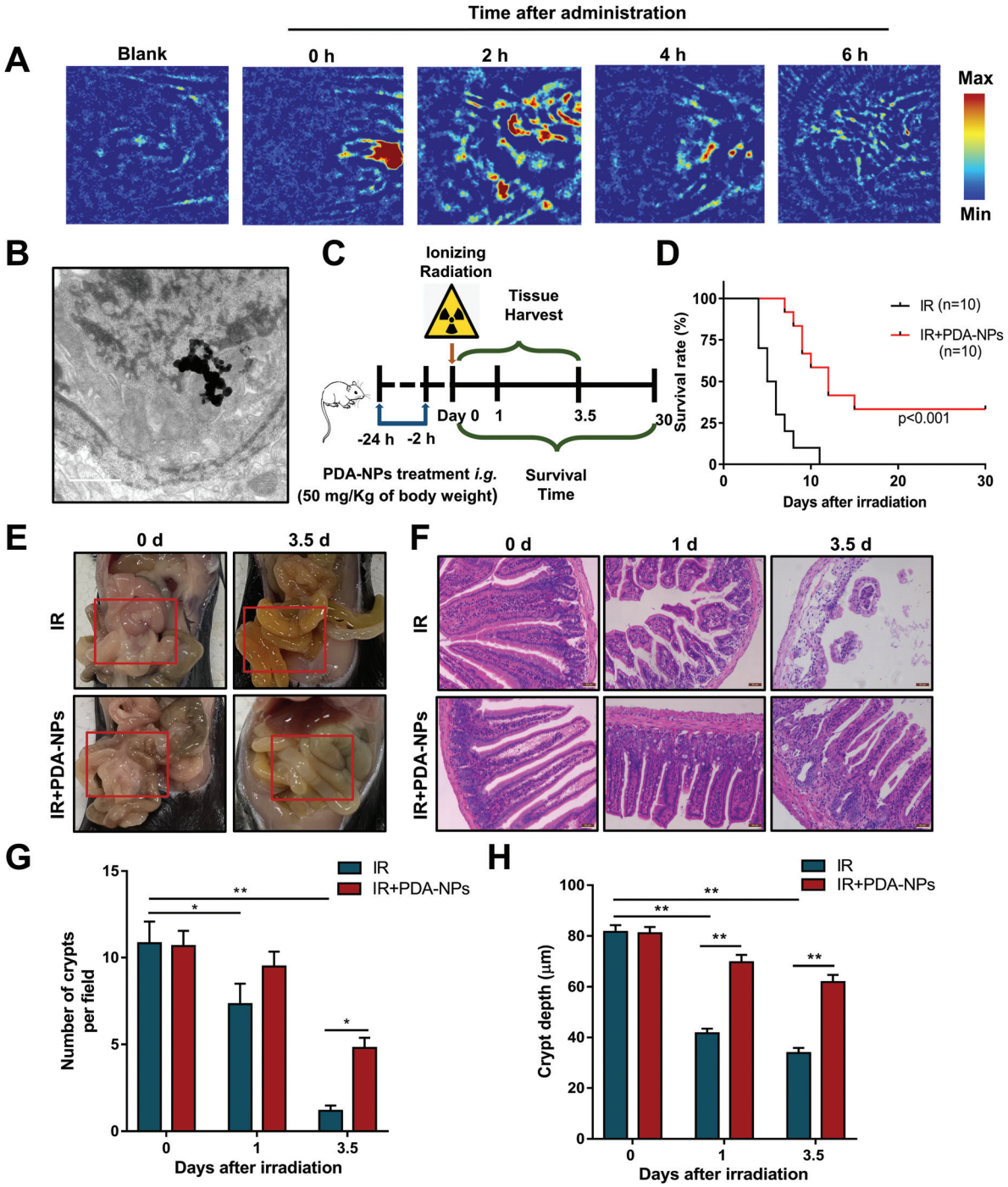

Fig. 2 PDA-NPs improved the survival and alleviated the intestine injury induced by TBI in Mice. (A) *In vivo* PAI after PDA-NP intragastric administration. (B) *In vivo* TEM images of the mice 2 h after PDA-NP intragastric administration (scale bar: 1 μm). (C) The pattern of PDA-NP administration treatment. (D) The anatomical appearance of intestine after 10 Gy TBI, $n = 3$ (E) H&E staining of the intestines after 10 Gy TBI (scale bar: 50 μm), $n = 3$. (F) Statistical graph of the number of crypts per view fields, $n = 6$. (G) Statistical graph of the depth of the crypt per view fields, $n = 15$. Data are expressed as mean ± SEM, $^{*}P < 0.05$, $^{**}P < 0.01$.

the outside of the intestinal wall, thinned the intestine and the intestinal mucosa, and led to a large amount of watery diarrhea (Fig. 2E). However, PDA-NP treatment alleviated the injury and maintained intestinal contents at a normal state. These phenomena were further confirmed by H&E staining (Fig. 2F). Compared with the control group, epithelial necrosis, villus length, inflammatory cell infiltration and crypt reduction were apparent in mice in the IR group (Fig. 2G and H). However, PDA-NP-treated mice showed less intestinal histopathological damage, increased epithelial thickness, more sur-

viving crypts, and higher villi. Therefore, we concluded that PDA-NPs alleviated intestinal injury induced by TBI in mice.

3.3 PDA-NPs protected intestinal homeostasis and function after TBI

The morphology and quantity of feces are important indices to judge intestinal function.[33] We examined changes in the morphology, quantity and weight of feces after IR. The feces in the IR group changed significantly (Fig. 3A), and the number (Fig. 3B) and weight (Fig. 3E) of feces at 0, 1, 3 and 7 days decreased gradually. Although the feces in the PDA-NP administration group also decreased, there was little difference in the overall number. FITC dextran in serum has been used as an index to evaluate intestinal paracellular permeability.[34] Dextran is a nondigestible polysaccharide with a molecular weight of 3 kDa to 2000 kDa. Once ingested orally, this fluorescent marker will pass through the gastrointestinal tract and the intestinal epithelium. The concentration of 10 kDa FITC

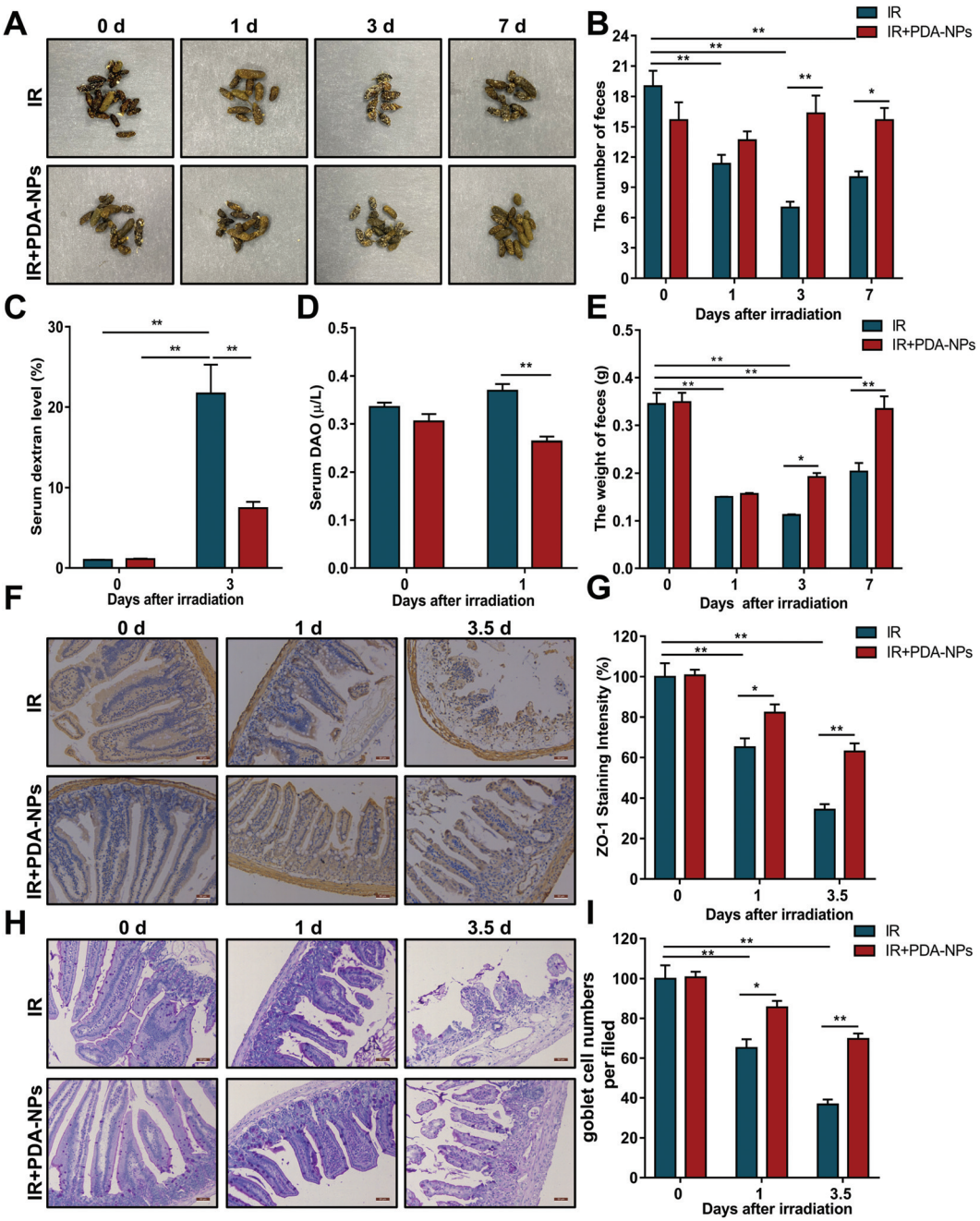

Fig. 3 PDA-NPs protected intestinal homeostasis and function after TBI. (A) The morphology of feces after 7.5 Gy TBI, n = 10; (B) the counts of feces, n = 3; (C) the mass of feces, n = 3; FITC-dextran (D) and DAO (E) levels in serum after 10 Gy TBI, n = 3. (F) The expression of ZO-1 after 10 Gy TBI (scale bar = 50 μm), n = 3. (G) Quantity of ZO-1 staining per view field, n = 3. (H) 10 Gy TBI followed by periodate Schiff (PAS) staining, n = 3. (I) The number of goblet cells per view fields, n = 3. Data are expressed as mean ± SEM, $^{*}P < 0.05$, $^{**}P < 0.01$.

dextran in serum can be readily measured by fluorimetry and used as a probe to measure intestinal epithelial cell paracellular permeability.[35] Compared with the IR group (Fig. 3C), PDA-NP treatment significantly reduced FITC dextran uptake in the serum ($P < 0.001$). Moreover, DAO in serum is usually regarded as an indirect indicator of intestinal permeability, which further verified that PDA-NPs could maintain the normal barrier function of the intestine (Fig. 3D). Epithelial barrier is the first line of defense in the gastrointestinal tract, preventing bacterial toxins from spreading to the intestinal mucosa and finally to the systemic circulation.[36] Tight junctions are highly specialized intercellular junctions that provide strong barrier function to the gastrointestinal epithelium.[37] Immunohistochemical analysis of the tight junction protein ZO-1 in the mouse small intestine was performed. Compared with the IR group, PDA-NPs alleviated the decrease in intestinal tight junction protein ZO-1 induced by IR (Fig. 3F and G). Goblet cells (GCs) are special epithelial cells that are distributed on many mucosal surfaces and play an important role in barrier maintenance by secreting mucus. In addition, GCs

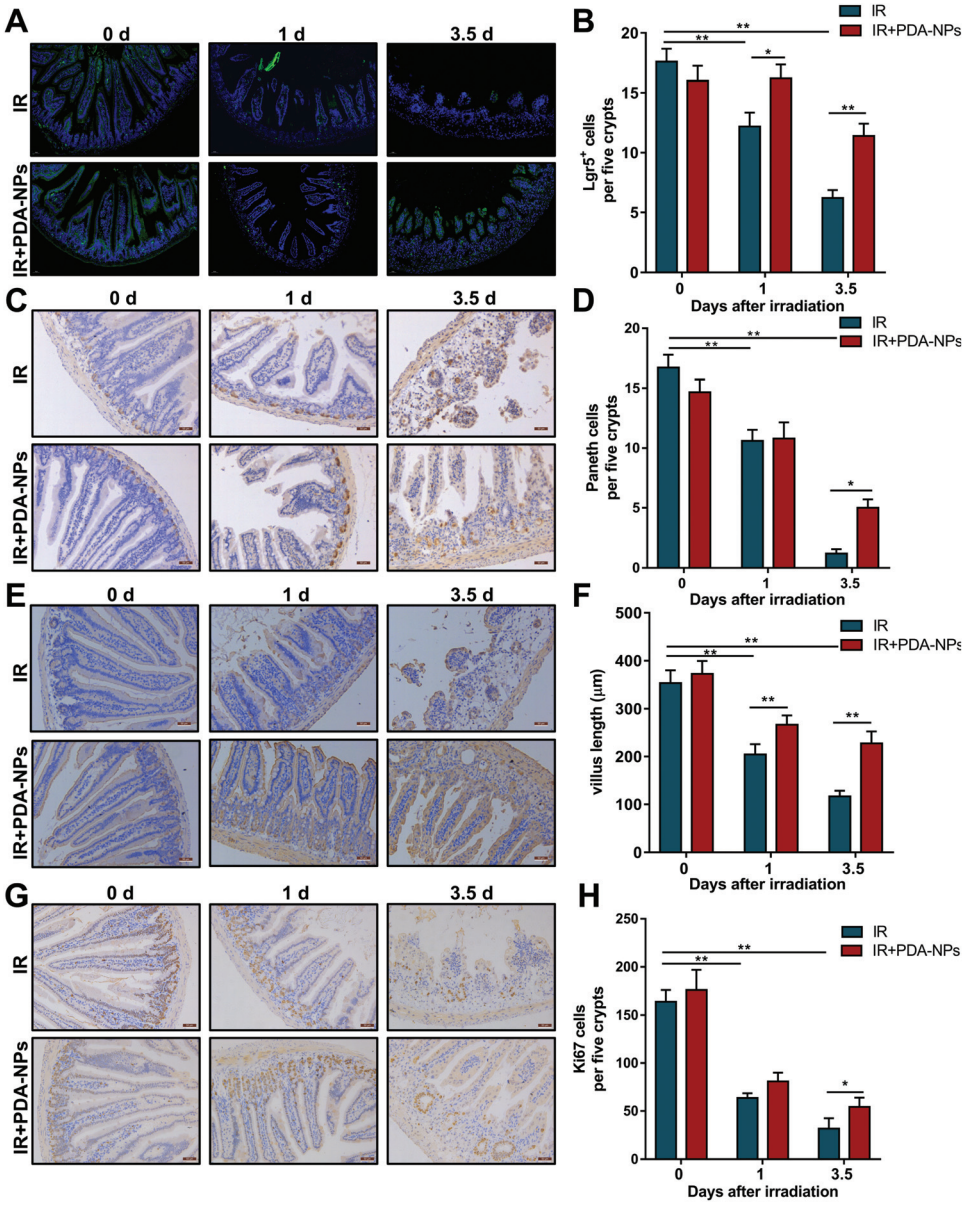

Fig. 4 PDA-NPs promoted the reservation and regeneration of ISCs after TBI. (A) The of FISH Lgr5$^+$ cells in crypts after 10 Gy TBI, n = 3. (B) The counts of Lgr5$^+$ cells in each per view field, n = 5. (C) Lysozyme IHC staining for Paneth cells of after 10 Gy TBI, n = 3. (D) The counts of Lysozyme$^+$ cells in per five crypts, n = 7. (E) Villin expression in intestines after10 Gy TBI (scale bar: 50 m), n = 3. (F) The counts of Villin + cells in each villus, n = 15. (G) The Ki67$^+$ cells in crypts after 10 Gy TBI, n = 3. (H) The counts of Ki67$^+$ cells in per five crypts, n = 5. Data were expressed as mean ± SEM, *$P < 0.05$, **$P < 0.01$.

secrete antibacterial proteins, chemokines and cytokines, which participate in innate immunity in addition to barrier maintenance.[38] The number of GCs decreased significantly to 55.5% at 1 day after IR (Fig. 3H and I), while PDA-NP administration significantly prevented this change; the number of GCs in the intestine of the PDA-NPs group was 93.8%, which indicated that PDA-NPs effectively prevented the decrease in GCs induced by IR. These results indicated that PDA-NPs might have a protective effect on IR-induced intestinal injury.

3.4 PDA-NPs promoted the preservation and regeneration of ISCs after TBI

Single Lgr5$^+$ ISCs can generate a 'mini intestine' *in vitro*, comprising all differentiated intestinal cell types.[8] When Lgr5$^+$ ISCs are lost, the number of progeny cells decreases as a consequence. To evaluate the effect of PDA-NPs on the proliferation and differentiation of crypts and clarify the role of PDA-NPs in the preservation and regeneration of intestinal cells in irradiated mice, ISCs (Lgr5$^+$), Paneth cells (Lysozyme$^+$), CBCs (Ki67$^+$) and intestinal cells (Villin$^+$) were stained by FISH or IHC. Paneth cells are secretory intestinal epithelial cells that produce lysozyme.[11] They are born in the proliferative crypt region and migrate upward and differentiate to maintain intestinal homeostasis. Villin, a tissue-specific actin binding protein, is involved in the formation of intestinal microvilli, which differentiate into functional cells.[39] We found that after 3.5 days of IR, the number of Lgr5$^+$ ISCs in the PDA-NP treatment group increased (Fig. 4A and B) and differentiated into more Paneth cells (Fig. 4C and D) and villous intestinal cells (Fig. 4E and F). CBCs are usually positive for the proliferation marker Ki67. Immunostaining of Ki67 recognizes proliferating cells, indicating that cells are in a circulating state and regenerating.[7] In PDA-NP treated mice, the expression of Ki67 increased compared with that in the IR group (Fig. 4G and H), indicating that intestinal cells recovered after IR-induced damage. Therefore, PDA-NPs might play a protective role against IR-induced intestinal injury by promoting the proliferation and differentiation of Lgr5$^+$ ISCs.

3.5 PDA-NPs suppressed apoptosis and pyroptosis in the intestine after TBI

During radiotherapy, the interaction between IR and the biological system leads to injury to ISCs, a large part of which is caused by the generation of free radicals or ROS. ROS attack

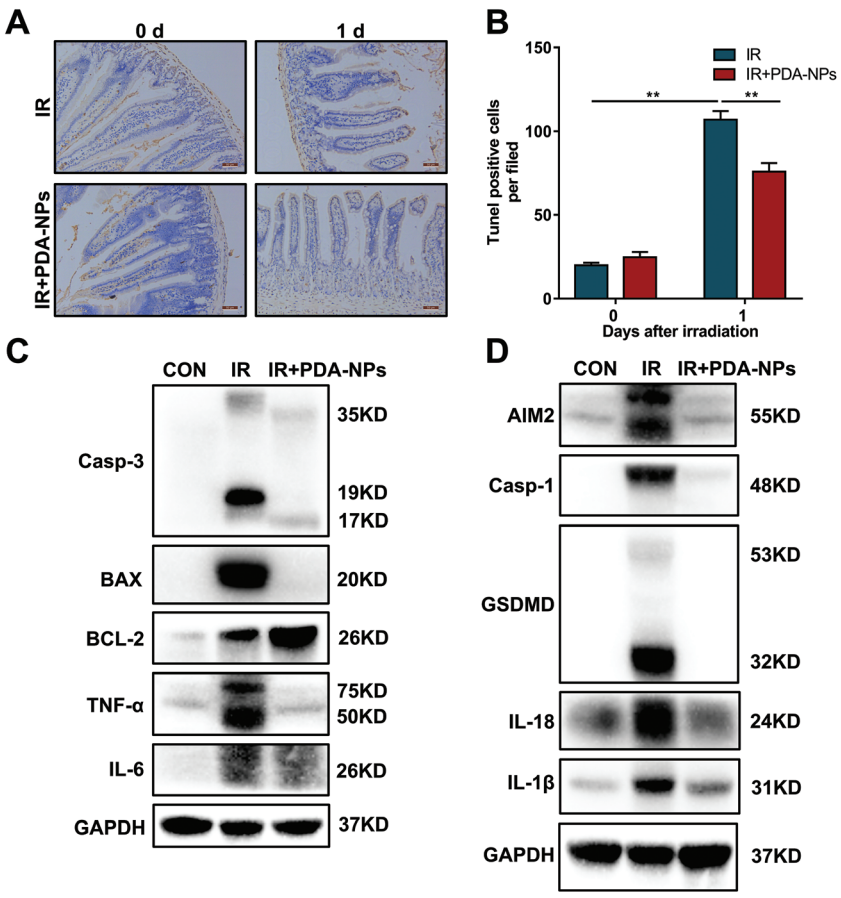

Fig. 5 PDA-NPs suppressed apoptosis and pyroptosis of intestines after TBI. (A) TUNEL staining after 10 Gy TBI, n = 3. (B) The number of TUNEL positive cells in per view field, n = 5. (C) Western blot analysis of the expression of apoptosis and inflammation proteins in 10 Gy TBI tissue lysates, n = 3. (D) Western blot analysis of the expression of pyroptosis proteins in 10 Gy TBI tissue lysates, n = 3. Data are expressed as mean ± SEM, $^*P < 0.05$, $^{**}P < 0.01$.

key macromolecules such as DNA, protein and membrane lipids in the cells, which damages $Lgr5^+$ ISCs and potentially causes cell dysfunction and death. This destroys the entire crypt–villus structure, and this change is irreparable.[30] Intestinal crypt epithelial cells are prone to apoptosis after IR exposure because of their fast proliferation. Apoptosis is a

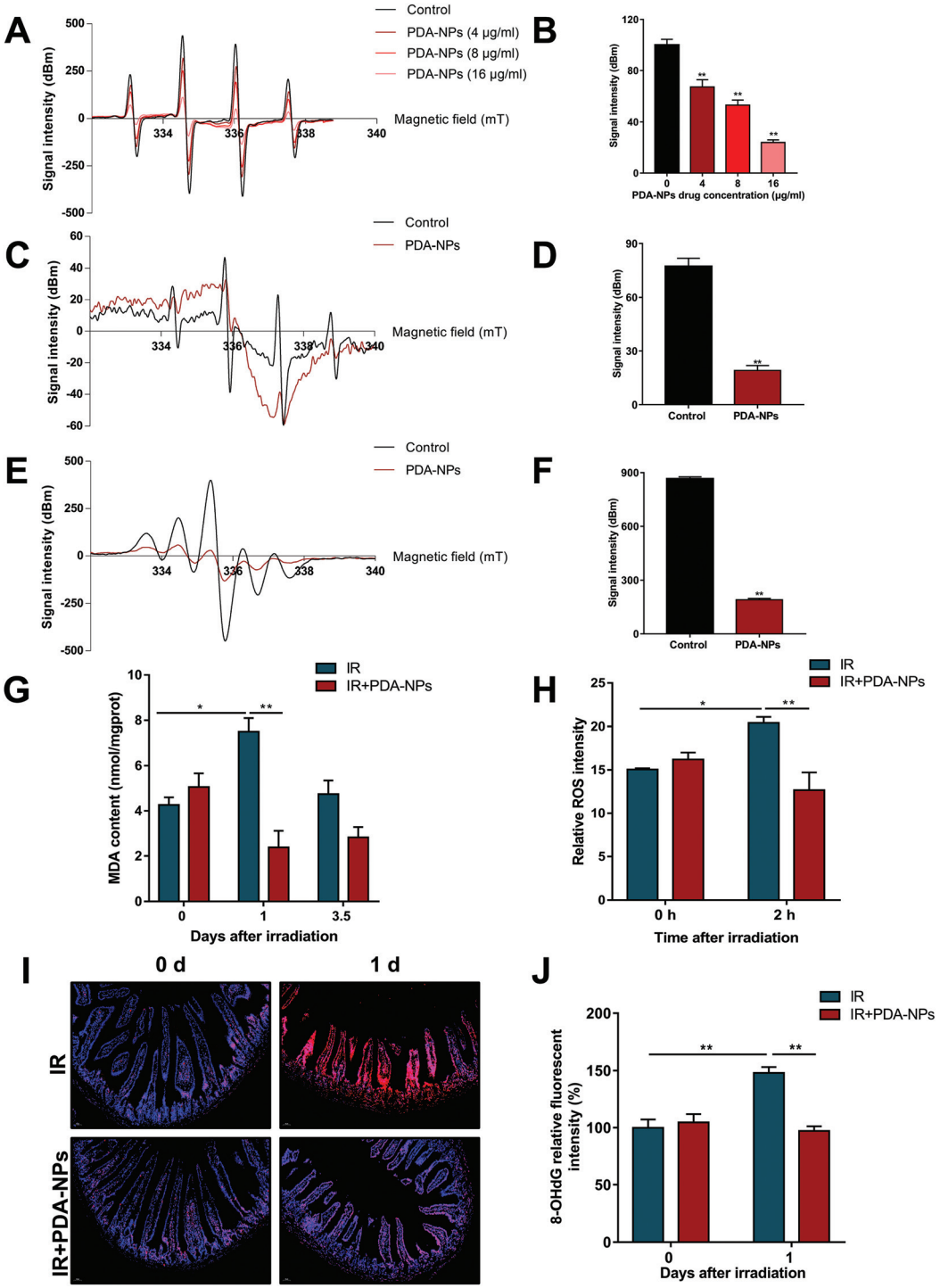

Fig. 6 PDA-NPs suppressed ROS generation and DNA damage of intestines after TBI. (A) ESR spectrum of $^{\cdot}OH$ captured by DMPO generated by Fenton reaction with different concentrations of PDA-NPs. (B) ESR peak histogram of $^{\cdot}OH$, $n = 3$. (C) ESR spectrum of $O_2^{\cdot-}$ captured by DMPO generated by Xan-XOD with PDA-NPs. (D) ESR peak histogram of $O_2^{\cdot-}$, $n = 3$. (E) ESR spectrum of DPPH with or without PDA-NPs. (F) ESR peak histogram of DPPH, $n = 3$. (G) MDA levels in the intestinal tissues were determined 1 and 3.5 days after 10 Gy IR, $n = 3$. (H) ROS levels in the HIEC cells were determined 2 h after 8 Gy IR, $n = 3$. (I) The representative 8-OHdG staining images after 10 Gy TBI (scale bar: 50 μm), $n = 3$. (J) Quantification of 8-OHdG positive cells in each per view field (400×), $n = 3$. Data were expressed as mean ± SEM, $^*P < 0.05$, $^{**}P < 0.01$.

major type of cell death induced by IR.[9] Radiation-mediated mitochondrial damage leads to a decrease in mitochondrial membrane potential, the activation of caspase-3 and the release of Cyto C. Bax, a death-promoting protein, is upregulated, while BCL-2, a death-inhibiting protein, is downregulated in this process. To evaluate the effect of PDA-NPs on IR-induced apoptosis, we monitored apoptosis in the mouse intestinal crypt epithelium 24 h after TBI (Fig. 5A and B). The number of apoptotic nuclei in the intestinal crypts of mice increased, and PDA-NP treatment reversed this phenomenon. Furthermore, after IR, the apoptosis-related proteins caspase-3 and Bax in intestinal tissue increased significantly, while the anti-apoptosis protein BCL-2 decreased.[40] In addition to apoptosis, pyroptosis, also known as inflammatory necrosis, is a newly proposed programmed cell death mode involved in oxidative stress. We also found that ionizing radiation upregulated caspase-1, which led to the cleavage of GSDMD and the activation of the pyroptosis pathway and promoted the maturation and release of the downstream cytokines IL-1β and IL-18.[41] Our research found that the pyroptosis-related proteins caspase-1, GSDMD, IL-1β and IL-18 increased significantly. These data indicated that PDA-NPs could ameliorate IR-induced intestinal injury by suppressing apoptosis and pyroptosis pathways (Fig. 5C and D). In addition, PCR and western blot results showed that the levels of intestinal inflammatory marker TNF-α was significantly increased in the IR group, which was reversed by PDA-NPs (Fig. 5C, D, and S 6†). These results were further verified in the following *in vitro* experiments (Fig. S 4 and 5†). HIEC were used to study the potential mechanism of PDA-NPs-mediated radiation protection. Firstly, we performed the CCK-8 assay to evaluate the effect of PDA-NPs on cell viability. PDA-NP treatment with concentration lower than 20 μg mL^{-1} showed no cytotoxic effect on the proliferation of HIEC cells (Fig. S 7†). Then, in order to determine the radioprotective effect of PDA-NPs, HIEC cells were pre-treated with 8 μg mL^{-1} PDA-NPs before 8 Gy IR, and the cell viability was measured (Fig. S 8†). The results showed that IR decreased cell viability, which was reversed by PDA-NPs. Therefore, PDA-NPs at a concentration of 8 μg mL^{-1} was used in subsequent experiments.

3.6 PDA-NPs suppressed ROS generation and DNA damage of intestines after TBI

DNA oxidative damage can lead to oxidative stress in cells (especially stem cells).[42] $O_2^{\bullet-}$ and $^{\bullet}OH$ are two major free radicals generated during IR. Free radical scavenging has been proved to be the most effective treatment of radiation protection.[43,44] ESR assay was performed to determine the scavenging ability of PDA-NPs on $O_2^{\bullet-}$ and $^{\bullet}OH$ radicals. As shown in the Fig. 6A–D, PDA-NPs behaved well in scavenging oxygen free radicals. The scavenging rate of $^{\bullet}OH$ free radicals increased with the PDA-NP concentration. We also detected that PDA-NPs had strong scavenging ability on DPPH free radical (Fig. 6E and F). In addition, the advantages of PDA-NPs not only lie in their efficient free radical scavenging ability, but also in their chemical stability in the gastrointestinal environment, which ensure the application of PDA-NPs in intestinal radiation protection. Meanwhile, the free radical scavenging ability of PDA-NPs in strong acid (pH = 2) was detected by ESR. It was found that PDA-NPs maintained free radical scavenging ability under strong acid conditions (Fig. S 9 and 10†). These results indicated that PDA-NPs not only have good chemical stability, but also maintain high free radical scavenging ability under strong acid condition. Therefore, PDA-NPs have proved effective in protecting the intestines from irradiation through the gastrointestinal delivery. MDA levels were detected to evaluate the oxidative stress level of intestine tissues. After IR, MDA level significantly increased, which indicated that IR induced oxidative damage to intestines. PDA-NP pre-treatment before IR effectively alleviated this phenomenon (Fig. 6G). Otherwise, we examined the ability of PDA-NPs to scavenge ROS in irradiated HIEC cells. The level of ROS in HIEC cells increased significantly after IR compared to sham-irradiated HIEC cells, while treatment with PDA-NPs effectively suppressed the IR-induced generation of ROS in HIEC cells (Fig. 6H). If $^{\bullet}OH$ radicals attack guanine bases in DNA, they would be converted to 8-OHdG.[45] The results of 8-OHdG staining showed that 10 Gy X-rays increased 8-OHdG in intestinal crypts at 1 day and 3.5 days, which was inhibited by PDA-NP treatment (Fig. 5I and J). Our study indicated that the nanomaterial PDA-NPs plays a key role in preventing IR-induced DNA damage by inhibiting the generation of 8-OHdG.

Our research suggested that PDA-NPs had a good protective effect on radiation enteropathy; PDA-NP treatment maintained the intestinal contents close to the normal state, increased the number of goblet cells in the small intestine, significantly reduced the uptake of FITC-dextran and DAO into the serum, alleviated the decrease in intestinal tight junction protein ZO-1 after IR, increased the $^{\bullet}OH$ scavenging rate with increasing drug concentration, decreased the formation of 8-OHdG, suppressed apoptosis and pyrolysis, and mitigated the inflammatory reaction in the intestinal epithelium after IR exposure.

4. Conclusion

PDA-NPs were prepared and characterized, and their efficacy and possible mechanisms of action in protecting against IR-induced intestinal injury were explored in this study. We confirmed that PDA-NPs showed favorable structural characteristics, prolonged the average survival time of irradiated mice, improved the structure of the intestinal epithelium and maintained intestinal barrier function after IR. Mechanistically, PDA-NPs prevented the depletion of $Lgr5^+$ ISCs, promoted the repair of intestinal structure and function, suppressed apoptosis and pyroptosis and alleviated DNA damage induced by ionizing radiation. Our study suggested that PDA-NPs may be developed as a potential radioprotective agent against IR-induced intestinal injury.

Abbreviations

IR	Irradiation
PDA-NPs	Polydopamine nanomaterials
ROS	Reactive oxygen species
ISCs	$Lgr5^+$ intestinal stem cells
TBI	Total body irradiation
ABI	Abdomen irradiation
HIEC	Human intestinal epithelial cell
DMPO	5,5-Dimethyl-1-pyrroline-*N*-oxide
DPPH	1,1-Diphenyl-2-picrylhydrazine
FISH	Fluorescence probe *in situ* hybridization
PAS	Periodate Schiff
$^{\bullet}OH$	Scavenger hydroxyl radicals
$O2^{\bullet-}$	Superoxide anions
8-OHdG	8-Hydroxy-2-deoxyguanosine
MDA	Malondialdehyde
PA	Photoacoustic
PAI	Photoacoustic imaging
DAO	Diamine oxidase
Xan	Xanthine
XOD	Xanthine oxidase

Author contributions

Shuhan Jia, Suhe Dong, and Heng Liu contributed equally to this work. Shuhan Jia carried out all biological experiments and wrote the first draft of the manuscript. Suhe Dong designed experiments and wrote the manuscript. Heng Liu provided the material and carried out the characterization. Huijie Yu, Zhongmin Chen and Sinian Wang analyzed and interpreted the data. Renjun Peng, Fengsheng Li, Jianjun Liu and Qisheng Jiang supervision and verification. All authors read and amended the draft, and gave final approval of the manuscript.

Ethics approval and consent to participate

The animal study was reviewed and approved by the Ethics Committee of the PLA Rocket Force Characteristic Medical Center.

Conflicts of interest

The authors confirm that there are no conflicts of interest.

Acknowledgements

The authors thank Xiaoli Lv for his professional and technical help, and also thank Dongshu Liu, Jing Ma and Ziqing Zhang for their help with this experiment. This work was supported by the Military Research Program (AEP17J001) and National Natural Science Foundation of China (31770914, 82003388, 81901872).

References

1 G. Delaney, *et al.*, The role of radiotherapy in cancer treatment: estimating optimal utilization from a review of evidence-based clinical guidelines, *Cancer*, 2005, **104**(6), 1129–1137.
2 M. Hauer-Jensen, J. W. Denham and H. J. Andreyev, Radiation enteropathy–pathogenesis, treatment and prevention, *Nat. Rev. Gastroenterol. Hepatol.*, 2014, **11**(8), 470–479.
3 A. K. Shadad, *et al.*, Gastrointestinal radiation injury: symptoms, risk factors and mechanisms, *World J. Gastroenterol.*, 2013, **19**(2), 185–198.
4 J. W. Denham, M. Hauer-Jensen and L. J. Peters, Is it time for a new formalism to categorize normal tissue radiation injury?, *Int. J. Radiat. Oncol., Biol., Phys.*, 2001, **50**(5), 1105–1106.
5 H.-J. Martin, J. W. Marjan Boermac, Q. Fud and J. W. Denhame, Radiation damage to the gastrointestinal tract: mechanisms, diagnosis, and management, *Curr. Opin. Support. Palliat. Care*, 2007, **1**(23–29), 1751–4258.
6 C. S. Potten, *et al.*, Characterization of radiation-induced apoptosis in the small intestine and its biological implications, *Int. J. Radiat. Biol.*, 1994, **65**(1), 71–78.
7 N. Barker, *et al.*, Identification of stem cells in small intestine and colon by marker gene Lgr5, *Nature*, 2007, **449**(7165), 1003–1007.
8 T. Sato, *et al.*, Single Lgr5 stem cells build crypt-villus structures *in vitro* without a mesenchymal niche, *Nature*, 2009, **459**(7244), 262–265.
9 X. Sheng, *et al.*, Cycling Stem Cells Are Radioresistant and Regenerate the Intestine, *Cell Rep.*, 2020, **32**(4), 107952.
10 H. Ireland, *et al.*, Cellular inheritance of a Cre-activated reporter gene to determine Paneth cell longevity in the murine small intestine, *Dev. Dyn.*, 2005, **233**(4), 1332–1336.
11 T. Sato, *et al.*, Paneth cells constitute the niche for Lgr5 stem cells in intestinal crypts, *Nature*, 2011, **469**(7330), 415–418.
12 D. Qi, *et al.*, Repair and regeneration of small intestine: A review of current engineering approaches, *Biomaterials*, 2020, **240**, 119832.
13 J. P. Heath, Epithelial cell migration in the intestine, *Cell Biol. Int.*, 1996, **20**(2), 139–146.
14 Y. Cheng, *et al.*, The protective effects of XH-105 against radiation-induced intestinal injury, *J. Cell. Mol. Med.*, 2019, **23**(3), 2238–2247.
15 D. Yohan and B. D. Chithrani, Applications of nanoparticles in nanomedicine, *J. Biomed. Nanotechnol.*, 2014, **10**(9), 2371–2392.
16 Y. Liu, *et al.*, Biomimetic manganese-eumelanin nanocomposites for combined hyperthermia-immunotherapy against prostate cancer, *J. Nanobiotechnol.*, 2022, **20**(1), 48.

17 Y. Lee, *et al.*, Bilirubin Nanoparticles as a Nanomedicine for Anti-inflammation Therapy, *Angew. Chem., Int. Ed.*, 2016, **55**(26), 7460–7463.
18 A. Kunwar, *et al.*, Melanin, a promising radioprotector: mechanisms of actions in a mice model, *Toxicol. Appl. Pharmacol.*, 2012, **264**(2), 202–211.
19 K. Y. Ju, *et al.*, Bioinspired polymerization of dopamine to generate melanin-like nanoparticles having an excellent free-radical-scavenging property, *Biomacromolecules*, 2011, **12**(3), 625–632.
20 R. Batul, *et al.*, Recent progress in the biomedical applications of polydopamine nanostructures, *Biomater. Sci.*, 2017, **5**(7), 1204–1229.
21 X. Bao, *et al.*, Polydopamine Nanoparticles as Efficient Scavengers for Reactive Oxygen Species in Periodontal Disease, *ACS Nano*, 2018, **12**(9), 8882–8892.
22 L. Li, *et al.*, A Broad-Spectrum ROS-Eliminating Material for Prevention of Inflammation and Drug-Induced Organ Toxicity, *Adv. Sci.*, 2018, **5**(10), 1800781.
23 C. W. Li, *et al.*, Antioxidant Nanotherapies for the Treatment of Inflammatory Diseases, *Front. Bioeng. Biotechnol.*, 2020, **8**, 200.
24 J. Hu, *et al.*, Polydopamine free radical scavengers, *Biomater. Sci.*, 2020, **8**(18), 4940–4950.
25 A. R. Bilia, *et al.*, Nanocarriers: A Successful Tool to Increase Solubility, Stability and Optimise Bioefficacy of Natural Constituents, *Curr. Med. Chem.*, 2019, **26**(24), 4631–4656.
26 K. H. Huynh, *et al.*, Synthesis, Properties, and Biological Applications of Metallic Alloy Nanoparticles, *Int. J. Mol. Sci.*, 2020, **21**(14), 51–74.
27 K. B. Narayanan and H. H. Park, Pleiotropic functions of antioxidant nanoparticles for longevity and medicine, *Adv. Colloid Interface Sci.*, 2013, **201–202**, 30–42.
28 M. M. Rageh, *et al.*, Melanin nanoparticles (MNPs) provide protection against whole-body -irradiation in mice via restoration of hematopoietic tissues, *Mol. Cell. Biochem.*, 2015, **399**(1–2), 59–69.
29 N. Huang, *et al.*, Multifunctional Electrochemical Platforms Based on the Michael Addition/Schiff Base Reaction of Polydopamine Modified Reduced Graphene Oxide: Construction and Application, *ACS Appl. Mater. Interfaces*, 2015, **7**(32), 17935–17946.
30 Y. Liu, *et al.*, Dopamine-melanin colloidal nanospheres: an efficient near-infrared photothermal therapeutic agent for in vivo cancer therapy, *Adv. Mater.*, 2013, **25**(9), 1353–1359.
31 S. Zhang, *et al.*, Terrylenediimide-Based Intrinsic Theranostic Nanomedicines with High Photothermal Conversion Efficiency for Photoacoustic Imaging-Guided Cancer Therapy, *ACS Nano*, 2017, **11**(4), 3797–3805.
32 P. K. Shukla, *et al.*, Rapid disruption of intestinal epithelial tight junction and barrier dysfunction by ionizing radiation in mouse colon in vivo: protection by N-acetyl-l-cysteine, *Am. J. Physiol.: Gastrointest. Liver Physiol.*, 2016, **310**(9), G705–G715.
33 N. A. Atanasov, *et al.*, Characterization of Train-Induced Vibration and its Effect on Fecal Corticosterone Metabolites in Mice, *J. Am. Assoc. Lab. Anim. Sci.*, 2015, **54**(6), 737–744.
34 L. M. Napolitano, *et al.*, The impact of femur fracture with associated soft tissue injury on immune function and intestinal permeability, *Shock*, 1996, **5**(3), 202–207.
35 A. Woting and M. Blaut, Small Intestinal Permeability and Gut-Transit Time Determined with Low and High Molecular Weight Fluorescein Isothiocyanate-Dextrans in C3H Mice, *Nutrients*, 2018, **10**(6), 685.
36 E. C. Martens, M. Neumann and M. S. Desai, Interactions of commensal and pathogenic microorganisms with the intestinal mucosal barrier, *Nat. Rev. Microbiol.*, 2018, **16**(8), 457–470.
37 N. Tajik, *et al.*, Targeting zonulin and intestinal epithelial barrier function to prevent onset of arthritis, *Nat. Commun.*, 2020, **11**(1), 1995.
38 K. A. Knoop and R. D. Newberry, Goblet cells: multifaceted players in immunity at mucosal surfaces, *Mucosal Immunol.*, 2018, **11**(6), 1551–1557.
39 R. Athman, D. Louvard and S. Robine, Villin enhances hepatocyte growth factor-induced actin cytoskeleton remodeling in epithelial cells, *Mol. Biol. Cell*, 2003, **14**(11), 4641–4653.
40 M. Almoiliqy, *et al.*, Cinnamaldehyde protects against rat intestinal ischemia/reperfusion injuries by synergistic inhibition of NF-kappaB and p53, *Acta Pharmacol. Sin.*, 2020, **41**(9), 1208–1222.
41 G. Li, *et al.*, A New Participant in the Pathogenesis of Alcoholic Gastritis: Pyroptosis, *Cell. Physiol. Biochem.*, 2018, **49**(1), 406–418.
42 T. T. Wang, *et al.*, *In vitro* studies on the antioxidant and protective effect of 2-substituted -8-hydroxyquinoline derivatives against H(2)O(2)-induced oxidative stress in BMSCs, *Chem. Biol. Drug Des.*, 2010, **75**(2), 214–222.
43 S. Tsuruoka, *et al.*, Radical scavenging reaction kinetics with multiwalled carbon nanotubes, *Carbon*, 2015, **83**, 232–239.
44 T. Siddiqui, *et al.*, Reactive oxygen species and anti-proteinases, *Arch. Physiol. Biochem.*, 2016, **122**(1), 1–7.
45 J. Lin, *et al.*, Folium Sennae protects against hydroxyl radical-induced DNA damage via antioxidant mechanism: an in vitro study, *Bot. Stud.*, 2014, **55**(1), 16.

